Hydrodeoxygenation of Guaiacol over Bimetallic Fe-Alloyed (Ni, Pt) Surfaces: Reaction Mechanism, Transition-State Scaling Relations and Descriptor for Predicting C-O Bond Scission Reactivity

Journal:	*Catalysis Science & Technology*
Manuscript ID	CY-ART-02-2018-000282.R1
Article Type:	Paper
Date Submitted by the Author:	07-Mar-2018
Complete List of Authors:	Liu, Xiaoyang; Shanghai University of Engineering Science, College of Chemistry and Chemical Engineering An, Wei; Shanghai University Of Engineering Science, Chemistry and Chemical Engineering Wang, Yixing; Shanghai University of Engineering Science, College of Chemistry and Chemical Engineering Turner, Christoffer; The University of Alabama, Chemical and Biological Engineering Resasco, Daniel; University of Oklahoma, School of Chemical, Biological and Materials Engineering

Hydrodeoxygenation of Guaiacol over Bimetallic Fe-Alloyed (Ni, Pt) Surfaces: Reaction Mechanism, Transition-State Scaling Relations and Descriptor for Predicting C-O Bond Scission Reactivity

Xiaoyang Liu,[a] Wei An,[a]* Yixing Wang,[a] C. Heath Turner,[b] Daniel E. Resasco[c]

[a]College of Chemistry and Chemical Engineering, Shanghai University of Engineering Science, Songjiang District, Shanghai 201620, China

[b]Department of Chemical and Biological Engineering, University of Alabama, Tuscaloosa, AL 35487-0203, United States

[c]School of Chemical, Biological and Materials Engineering and Center for Biomass Refining, University of Oklahoma, Norman, OK 73019, United States

*E-mail: weian@sues.edu.cn

KEYWORDS: deoxygenation, guaiacol, bimetallic Fe alloy, C-O bond length, density functional theory

ABSTRACT: We examine initial hydrodeoxygenation (HDO) of guaiacol on bimetallic NiFe(111) and PtFe(111) using density functional theory. Our results show that on NiFe(111), the direct C_{aryl}–O bond breaking and dehydrogenation are preferred over hydrogenation, while on PtFe(111), hydrogenation/dehydrogenation are preferred over C_{aryl}–O bond breaking. Catechol is the major product of guaiacol-HDO on both Fe-alloyed surfaces via dehydrogenation of methoxy OCH_3 followed by O-CH_2 bond scission being promoted by oxophilic-Fe alloying. In comparison, the removals of oxo-functional group of guaiacol (i.e., $C_{aryl(\alpha)}$-OH, $C_{aryl(\beta)}$-OCH_3 and $C_{aryl(\beta)}$O-CH_3 bond breakings) on both Fe-alloyed surfaces are more facile energetically than those on monometallic Ni(111) and Pt(111) owing to oxophilic Fe active surface sites. It is confirmed that the C-O bond length of adsorbed intermediates can serve as a good descriptor for predicting C-O bond scission reactivity of the lignin-derived phenolic compounds on metal surfaces depending on C-O bond scission types.

1. INTRODUCTION

Hydrodeoxygenation (HDO) has been regarded as the most effective way to upgrading bio-oil by removing the oxygen-containing group from the highly complex mixture (such as acids, esters, alcohols, furfural, aldehydes and lignin-derived phenolic compounds).[1-7] Some phenolic model compounds with diverse O-containing functional groups, such as phenol,[8-16] cresol,[17-26] anisole[27-30] and guaiacol[29-49] have been employed in both experimental and theoretical studies. Guaiacol, or 2-methoxy-phenol [$C_6H_4(OH)(OCH_3)$], has been regarded as the star model compound due to its typical C-O bonds (i.e., C-OH, C-OCH_3 and O-CH_3) popular in phenolics. In a HDO process, various products of C-O bond breaking can be produced such as phenol [$C_6H_5(OH)$], catechol [$C_6H_4(OH)_2$], anisole [$C_6H_5(OCH_3)$], which may further serve as the reaction intermediates for forming the final desired product of benzene (C_6H_6) or alkybenzene, e.g., toluene ($C_6H_5CH_3$), via alkylation and transalkylation catalyzed by acidic sites on metal oxides or zeolite. This leads to the enhanced complexity for understanding the mechanistic aspects of guaiacol HDO.

Many catalyst systems have been shown to be active for guaiacol HDO. For example, Olcese et al., compared gas-phase HDO of guaiacol over Fe/SiO_2 and Co/SiO_2, and they revealed that Fe/SiO_2 catalyst is highly selective for deoxygenation products (i.e., benzene, toluene).[35] The supports and iron loading also play an important role in determining the product selectivity, in which phenol and cresols were mainly observed on 10wt% Fe supported on activated carbon than Fe/SiO_2.[34] Chiu and Rösch[49] reported a DFT study on the sequential step-by-step C-O bond breaking of guaiacol on Ru(0001) surface, where the dehydrogenation of hydroxyl is initiated followed by the removal of methyl group (CH_3) from the methoxy moiety (OCH_3) to yield catecholate followed by the oxo-groups being replaced by H, yielding phenolate and finally benzene. Moreover, the breaking of the aromatic bonds C_{aryl}–O needs a higher barrier than dehydrogenation of hydroxyl group or methyl group. Meanwhile, Lu and Heyden[46, 47] have systematically investigated guaiacol HDO on Pt(111) and Ru(0001) using DFT calculations and microkinetic modeling, suggesting that at 573 K, catechol is the preferred product on Pt with any phenol or benzene production via deoxygenation at least 4 orders of magnitude slower than catechol formation, whereas the dominant HDO pathway on Ru proceeds via O–H bond scission, i.e., $C_6H_4(OH)(OCH_3) \rightarrow C_6H_4(O)(OCH_3)$, followed by dehydrogenation of the methoxy group (OCH_3) to $C_6H_4(O)(OC)$, and then decarbonylation to C_6H_4O, which is further hydrogenated to phenol. Furthermore, Lee et al.[45] investigated guaiacol-HDO mechanism on Pt(111) and established new Brønsted-Evans-Polanyi (BEP) relations, which are applied to construct the potential energy surface of guaiacol HDO to form catechol. They found that catechol is mainly produced via dehydrogenation of the methoxy group followed by the CH_x ($x<3$) removal and hydrogenation of the ring.

Bimetallic catalysts are in particular of interest for selective C-O bonds breaking due to their tunable chemical and physical properties mainly through geometric (or ensemble), electronic (or ligand), and bifunctional effects.[3-5] These effects can lead to numerous beneficial outcomes such as increasing catalytic activity, modifying the selectivity, and improving catalyst stability under experimental HDO conditions. For example, bimetallic Pt-Sn/Inconel and Pt-Sn/CNF/Inconel were able to fully deoxygenate guaiacol to form toluene and benzene due to the oxophilicity of tin.[30] Sun et al. found that the carbon-supported Pd–Fe catalysts enhanced the activity of guaiacol HDO without promoting ring saturation or ring opening reactions and concluded that such enhancement is originated from the introduction of oxophilic Fe atoms into Pd matrix.[48] The similar effect of oxophilic Mo was also found for CoMo catalysts to promote guaiacol HDO.[50] In addition, it was found that anisole HDO over different metal catalysts (Pt, Ru, Fe)[27] exhibited a linear relationship between oxophilicity of Pt(111), Ru(0001) and Fe(110) and the intrinsic energy barrier for hydrogenation and

deoxygenation of phenoxy. On MO_x-supported Pd (MO_x = SiO_2, Al_2O_3, TiO_2, ZrO_2, CeO_2, and $CeZrO_2$),[8] phenol HDO also exhibited a correlation between the deoxygenation activity and the interaction strength of phenolic-O species with oxophilic sites of supports. Along this line, the reaction energy for demethoxylation or dehydroxylation of guaiacol has been well correlated with the dissociative O_2 adsorption on ten Ti and Ni based ceramic surfaces (TiC, TiN, TiO_2, TiS_2, TiP and Ni_3C, Ni_3N, NiO, Ni_3S_2, Ni_2P), while hydrogenation of adsorbed benzyne to form benzene can be well predicted based on the dissociative H_2 adsorption.[51] Consequently, it is expected that a catalyst containing the high oxophilicity component with the low activation capability to phenyl ring would be highly selective to deoxygenation reaction of phenolics.

For better screening the effective catalysts for upgrading lignin-derived phenolics, it is essential to understand the mechanistic aspects of the removal of oxygen-containing groups on bimetallic catalysts, in particular, via direct deoxygenation (DDO) by the activation of C-O bonds. In this work, we systematically investigated guaiacol-HDO mechanism on the bimetallic Fe-alloyed (Ni, Pt) surfaces, namely, NiFe(111) and PtFe(111), with a focus of identifying an effective descriptor for C-O bond scission reactions in guaiacol HDO. We proposed a reaction scheme for possible deoxygenation of guaiacol on bimetallic surface (i.e., NiFe and PtFe), based on the types of C-O bond scission in different functional groups of guaiacol: (1) Dehydroxylation to form anisole via route (i) direct $C_{aryl(\alpha)}$-OH bond scission (DDO), (ii) hydrogenation of $C_{aryl(\alpha)}$ followed by $C_{aliphatic(\alpha)}$H-OH bond scission, (iii) dehydrogenation of hydroxyl followed by C-O bond scission; (2) Demethylation to catechol via route (i) direct O-CH_3 bond scission, (ii) dehydrogenation of methoxy group followed by O-CH_2 bond scission; (3) Demethoxylation to form phenol via route (i) direct $C_{aryl(\beta)}$-OCH_3 bond scission (DDO), (ii) hydrogenation of $C_{aryl(\beta)}$ followed by $C_{aliphatic(\beta)}$H-OCH_3 bond scission. Note that the routes of transhydrogenation on the phenyl ring and metal-assisted tautomerization on bimetallic Fe-alloyed (Ni, Pt) surfaces are excluded from our proposed scheme due to their much higher barriers based on our previous study on NiFe(111).[26]

Scheme 1. Proposed reaction scheme for possible hydrodeoxygenation of guaiacol on bimetallic surface[a]

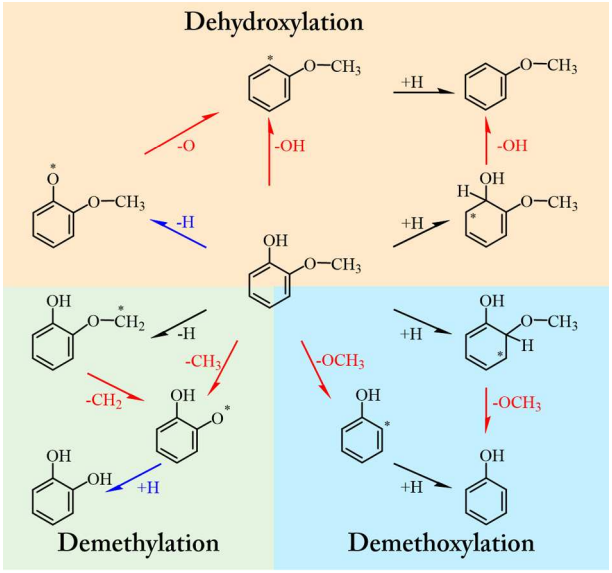

[a]: C-O scission: red, C-H scission or C-H formation: black, O-H scission or O-H formation: blue.

2. METHODS

All calculations were performed by using the periodic density functional theory (DFT) as implemented in the Vienna ab-initio simulation package (VASP).[52, 53] The Perdew-Burke-Ernzerhof (PBE) exchange-correlation functional[54] and the Projector Augmented Wave (PAW) method for describing the electron-ion interactions[55, 56] were adopted. The four-layer close-packed $p(4\times4)$ NiFe(111) and PtFe(111) slabs with a 14 Å vacuum region were built, in which the top two layers and adsorbates were relaxed while the bottom two layers were fixed at their optimized bulk positions of homogeneous alloy (NiFe $L1_0$alloy:[24, 57] $a = c$ = 3.553 Å, b = 3.582 Å; PtFe $L1_0$alloy:[58] $a = c$= 3.862 Å, b = 3.764 Å). The calculated lattice constants are close to the experimental values.[59] A 3×3×1 k-point grid generated with the Monkhorst-Pack scheme[60] was used to sample the first Brillouin zone and an energy smearing of 0.1 eV using the first-order Methfessel–Paxton scheme[61] was employed to speed up the convergence. An energy cutoff of 400 eV and the conjugate gradient algorithm was used in optimization with the convergence threshold of 10^{-4} eV in total energy and 0.02 eV/Å in Hellmann-Feynman force on each atom. Improved dimer method (IDM) was employed to calculate the activation barriers for various elementary-step reactions.[62, 63] The validity of calculation setups were detailed in our previous study.[26]

We denote aromatic adsorbates derived from HDO of guaiacol by the label x (x = 1 – 11), and a schematic representation of all structures studied is shown in Figure 1. The binding energy (*BE*) for reactant, stable intermediate, and product is defined as *BE* = *E*(ads/slab) – *E*(slab) – *E*(gas-phase), in which *E*(ads/slab), *E*(slab), and *E*(gas-phase) denote the total energy of adsorbate/slab, clean slab, and gas-phase molecule, respectively. The binding energies for reactant (guaiacol) and secondary products (anisole, catechol and phenol) were also calculated using optB88-vdW exchange-correlation functional[64, 65] with the correction of van der Waals (vdW) interactions (Table 1).

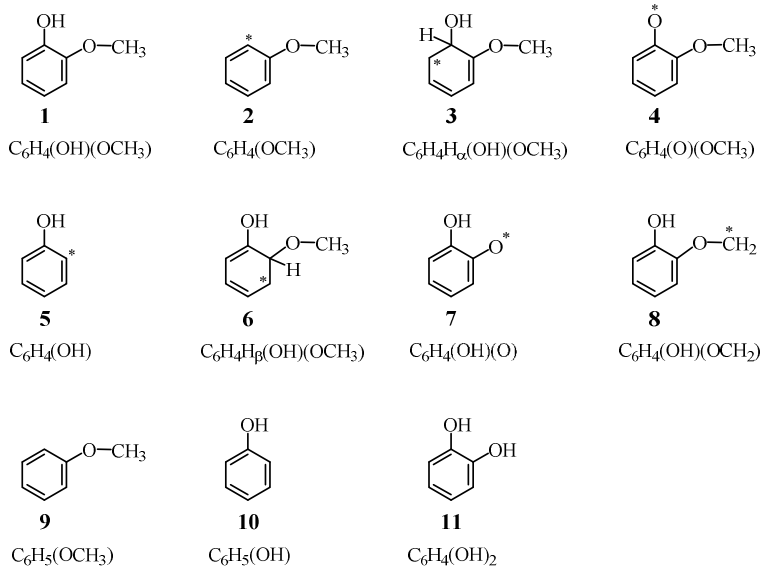

Figure 1. Schematic representation of structural formulas of the reactants, stable intermediates (derived from the probable reaction pathways shown in Scheme 1) and products under study, where * denotes one unpaired electron. H_α and H_β denote hydrogen atom bonding to the α-carbon (–OH) and β-carbon ($-OCH_3$), respectively.

3. RESULTS AND DISCUSSION

3.1. Adsorption of Guaiacol, Anisole, Catechol and Phenol on NiFe(111) and PtFe(111). The adsorption sites across the two threefold hollow sites (fcc and hcp) have been identified as the most stable sites for phenolic compounds

(e.g., guaiacol, anisole, cresol and phenol) and their adsorbed intermediate derivatives on metallic surfaces, such as Pt(111),[11, 14, 27, 45, 46] Pd(111),[11, 66] Ru(0001),[27, 47] Ni(111),[24, 26, 67] Fe(110),[24, 27, 66] as well as NiFe(111)[24, 26] and PdFe(111).[48] Four combinations (drawn in rhombus) of two threefold hollow sites can be seen for the adsorption of aromatic adsorbates on NiFe(111).[26] We calculated the adsorption of guaiacol [Figure 2(a)], anisole, phenol and catechol at the most stable adsorption site on NiFe(111) and PtFe(111) surfaces [Figure 2(b)] using Ni(111) and Pt(111) as references (Table 1 and Table S1). The adsorption energies of phenolics model compounds is approximately in the order of Pt(111) > Ni(111) ≈ NiFe(111) > PtFe(111). The calculated charge density difference isosurfaces demonstrated that the main interaction between guaiacol and the catalytic surface is via phenyl-metal binding, as indicated by the charge density accumulation [Figure 2(c)(d) and Figure S1], regardless of the adsorption sites. Two types of bonding can be identified as σ-type bonds (C3 and C6 with charge-depleted Fe atoms) and π-type bonds (C1=C2 and C4=C5 with charge-accumulated Ni or Pt atoms) between the aromatic ring and the surface activity sites. The calculated Bader charges indicate that the average charge transfer to each surface Ni atom and Pt atom owing to Fe alloying is 0.27 e^- and 0.63 e^- on NiFe(111) and PtFe(111), respectively, resulting in the lowering of Ni and Pt d-band center with respect to pure Ni and Pt (Figure 3). This also suggests the upmost surface of NiFe(111) and PtFe(111) is inhomogeneous and polarized in electron charge. Another important change induced by Fe alloying is the slight lattice expansion for NiFe alloy (i.e., 0.88% increase in a and c direction, 1.70% increase in b direction) with respect to Ni and the lattice contraction for PtFe alloy (i.e., 1.60% decrease in a and c direction, 4.10% decrease in b direction) with respect to Pt. This can lead to the slight Ni 3d-band center lifting and the slight Pt 4d-band center lowering, respectively. Overall, Ni 3d-band center of NiFe(111) is lowered to -1.56 eV from -1.26 eV of Ni(111), while Pt 4d-band center of PtFe(111) is lowered to -2.44 eV from -2.21 eV of Pt(111). An intimate bonding interaction of Ni-Fe and Pt-Fe is evident within NiFe and Pt-Fe alloy, respectively, resulting in the stabilization of the formed alloy and the enhancement of resistance to oxidation with respect to pure Fe.

From Figure 4, one can see that there exist two linear regimes for binding energy (*BE*) of phenolics versus d-band center of (i) total surface atoms [Figure 4(a)], and (ii) surface Ni and Pt atoms [Figure 4(b)], which are mainly attributed to π-type bonding. The trends comply with d-band model that as d-band centers are shifted upward towards Fermi level, the binding strength of phenolics is enhanced, however, the exception includes d-band center of surface Fe atoms [Figure 4(c)], which are mainly attributed to σ-type bonding. The adsorptions strength of phenolics are also dropped from the linear trend on Pt(111), which is known as nearly fully occupied d-band (mainly d^9 and d^{10} metals) substrate, and wherein, Pauli repulsion between adsorbate states (mainly cyclic continuous π-bond of phenyl ring having almost completely filled valence shell) and metal–states can be dominant that the stronger binding will be accompanied by larger binding distance and lower d-band center.[68] Indeed, guaiacol adsorption on Pt(111) yields *BE* of -2.00 eV with binding distance of Ni-C_{aryl}: 2.27 Å /2.16 Å (π-type /σ-type), contracting that on Ni(111) where *BE* = 1.76 eV, Ni-C_{aryl}= 2.11 Å /2.07 Å (π-type /σ-type). This explains the unusual observation that the substrates with higher d-band center bind the adsorbate less strongly than the substrates with lower energy of d-electrons, resulting in the trend of adsorption strength deviated from the d-band model. The Fe-alloying with Pt has changed the filling states of Pt making it behavior more like half-filled 3d metals thereby following d-band model.

Table 1. Binding energies (*BE*, in eV) for surface species of reactants and products adsorbed on Ni(111), NiFe(111), Pt(111) and PtFe(111)

BE (eV)	Ni(111)	NiFe(111)	Pt(111)	PtFe(111)
1 guaiacol	-1.76	-1.82	-2.00	-1.39
9 anisole	-1.82	-1.83	-1.99	-1.45
10 phenol	-1.83	-1.72	-2.02	-1.36
11 catechol	-1.83	-1.80	-1.89	-1.21

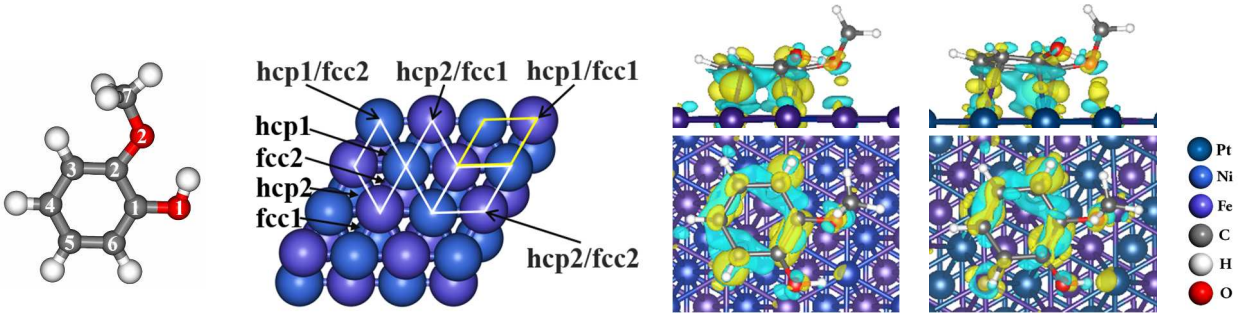

(a) (b) (c) (d)

Figure 2. (a) Optimized gas-phase guaiacol structure with C and O positions labeled; (b) Four combinations (rhombus) of two threefold hollow sites (i.e., fcc and hcp) for the adsorption of aromatic adsorbates on NiFe(111) and PtFe(111) surfaces, where 1 and 2 represent the number of Fe atoms in one threefold hollow site (e.g., hcp1/fcc1: one Fe atom in hcp and fcc site each, which is the most favored site for phenolic adsorption illustrated in yellow line); (c) and (d) Side view (top) and top view (bottom) of the three-dimensional isosurfaces of charge density difference ($\Delta\rho$) for adsorbed guaiacol at hcp1/fcc1 site of NiFe (111) and PtFe(111). Yellow and cyan isosurfaces (0.004 e/Bohr^3) represent the charge accumulation (i.e., gain of electron density) and the charge depletion (i.e., loss of electron density) in the space, following the definition: $\Delta\rho = \rho_{(slab+ads)} - \rho_{(slab)} - \rho_{(ads)}$.

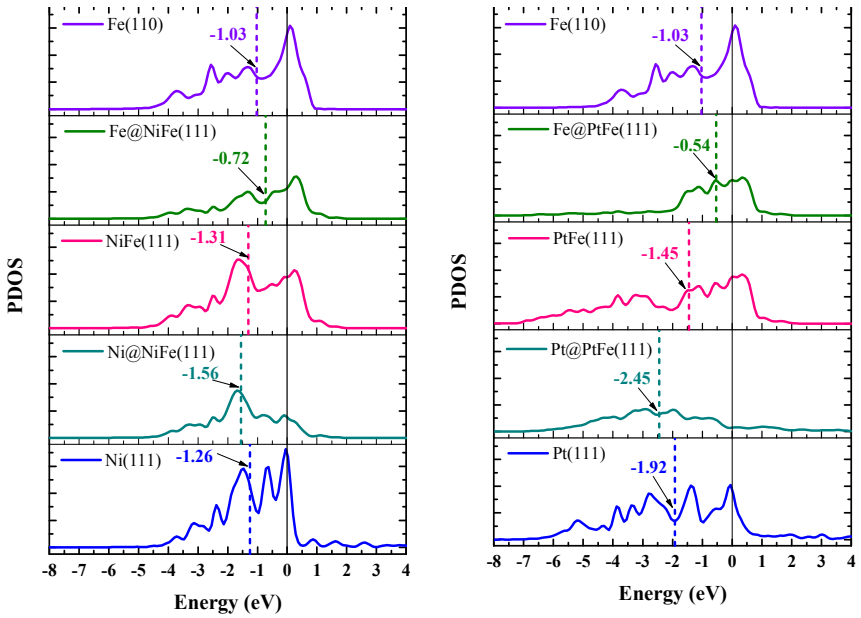

(a) NiFe(111) (b) PtFe(111)

Figure 3. Projected density of states (PDOS) for surface atoms of NiFe(111) and PtFe(111). Black line: Fermi level. Dashed line: d-band center of 3d states.

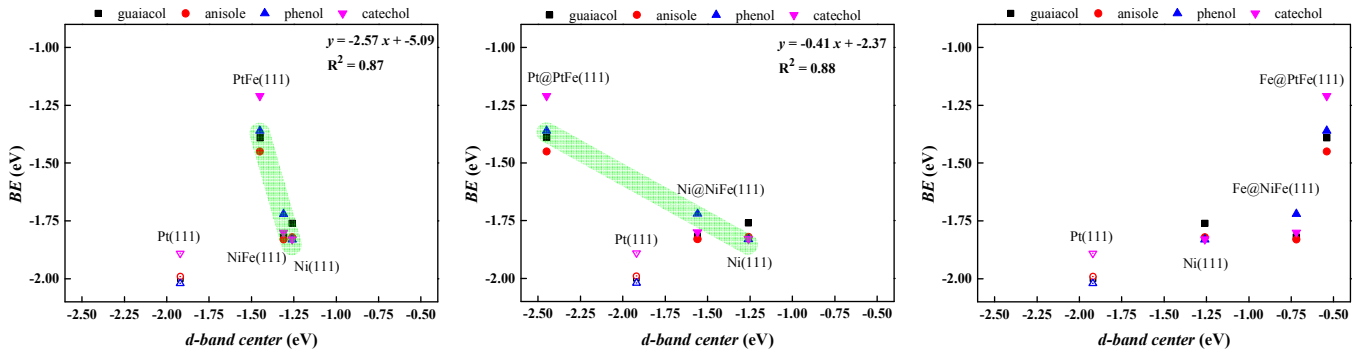

Figure 4. Plots of binding energy (*BE*) for guaiacol, anisole, phenol and catechol on NiFe(111) and PtFe(111) versus d-band center projected on (a) total surface atoms, (b) Ni and Pt surface atoms, (c) Fe surface atoms, using Ni(111) and Pt(111) as references. Labels are as in Figure 3.

3.2. Reaction Mechanism of Guaiacol to Anisole, Catechol and Phenol on NiFe(111) and PtFe(111).

3.2.1 Dehydroxylation of Guaiacol to Anisole. We first examined the three reaction pathways of dehydroxylation of guaiacol to anisole, as shown in Figure 5 and Figure S2. It can be seen that on NiFe(111), route (i) the direct $C_{aryl(\alpha)}$-OH bond scission of $C_6H_4(OH)(OCH_3)$(**1**), guaiacol, subsequently followed by hydrogenation to form $C_6H_4(OCH_3)$ (**2**), anisole, is the most favored one (E_a: 1.42 eV), as compared to route (ii) the selective hydrogenation of $C_{aryl(\alpha)}$ to $C_6H_4H_\alpha(OH)(OCH_3)$ (**3**) (E_a: 1.51 eV) and then CH-OH bond scission (E_a: 0.84 eV), and route (iii) the dehydrogenation of hydroxyl (E_a: 0.50 eV) and then C-O bond scission of deoxygenation (E_a: 1.80 eV), while on PtFe(111), route (ii) the hydrogenation of $C_{aryl(\alpha)}$ (E_a: 1.19 eV) and then CH-OH bond scission (E_a: 0.76 eV) is the most favored one followed by route (iii) the dehydrogenation of hydroxyl (E_a: 0.85 eV) and then C-O bond scission (E_a: 1.87 eV), and route (i) the direct $C_{aryl(\alpha)}$-OH bond scission of guaiacol (E_a: 2.05 eV). Moreover, it is notable that H-assisted CH-OH bond scission is much more facile than the direct $C_{aryl(\alpha)}$-OH bond scission on either NiFe(111) or PtFe(111), supported by our rational that C-OH bond length is closely correlated with the activation of C-O bond (see Section 3.4). Based on the calculated activation barriers for the rate determining step (RDS) of each route, we predict that the formation of anisole is more facile on PtFe(111) than NiFe(111) (E_a: 1.19 eV vs 1.42 eV). Note that dehydrogenation of hydroxyl of guaiacol, i.e., OH → O is the more likely to be the first step in HDO on both NiFe(111) and PtFe(111) considering their lowest activation barrier, similar to that (E_a: 0.46 eV) on Pt(111),[45] however, the subsequent steps of $C_{aryl(\alpha)}$-O scission are blocked due to much higher barrier, i.e., 1.80 eV on NiFe(111) and 1.87 eV on PtFe(111), making route (iii) less likely to occur on two alloys. This discrepancy of the preferred route of dehydroxylation of guaiacol to anisole on NiFe(111) and PtFe(111) can be explained by (1) the more oxophilicity of Ni than Pt, making Fe-alloyed Ni highly active for the direct removal of hydroxyl OH, and (2) the more hydrogenated functionality of Pt than Ni,[14] making Fe-alloyed Pt preferentially hydrogenating $C_{aryl(\alpha)}$ as the starting step. The similar results were also reported on oxophilic Fe(110),[10] and Ru/TiO_2,[12] where the direct C-OH bond scission is the dominant deoxygenation pathway for HDO of phenol and m-cresol on Ru(0001).[20]

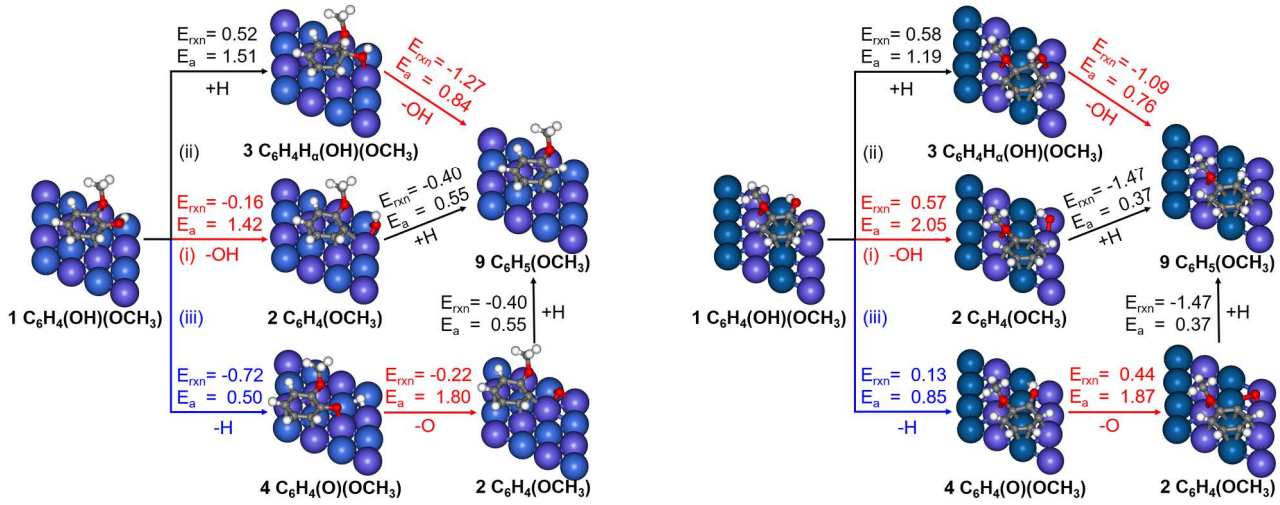

Figure 5. Reaction network for dehydroxylation of guaiacol to anisole over (a) NiFe(111) and (b) PtFe(111). Route (i): direct $C_{aryl(\alpha)}$-OH bond scission (middle panel); Route (ii): dehydrogenation of hydroxyl followed by C-O bond scission (lower panel); Route (iii): hydrogenation of $C_{aryl(\alpha)}$ followed by C-OH bond scission (upper panel). The reaction energy (E_{rxn}) and activation energy (E_a) with zero-point energy correction are listed. Red: C-O scission; Black: C-H scission or C-H formation; Blue: O-H scission and formation.

***3**.2.2 Demethoxylation of Guaiacol to Phenol.* We then examined the two reaction pathways of demethoxylation of guaiacol to phenol, as shown in Figure 6 and Figure S2. The direct deoxygenation route (i) proceeds via the direct C-OCH_3 bond scission at $C_{aryl(\beta)}$ of **1** to form $C_6H_4(OH)$ (**5**) followed by H-addition of $C_{aryl(\beta)}$ on the unsaturated ring to yield $C_6H_5(OH)$ (**10**), phenol. We excluded demethoxylation step via dehydrogenation of OCH_3 group, because the dehydrogenation will further promote the breaking of the formed O-CH_2 bond but make little effect on $C_{aryl(\beta)}$ -OCH_2 bond breaking as observed on Pt(111)[45, 46] and Ru(0001).[47] On NiFe(111), route (i) the direct $C_{aryl(\beta)}$-OCH_3 bond scission (E_a: 1.37 eV) of **1** is more favored than route (ii) the hydrogenation of $C_{aryl(\beta)}$ (E_a: 1.54 eV) of **1** to yield $C_6H_4H_\beta(OH)(OCH_3)$ (**6**), followed by CH_β-OCH_3 bond scission (E_a: 0.91 eV) to form phenol, whereas on PtFe(111), route (ii) (E_a: 1.08 eV and E_a: 0.91 eV) is more favored than route (i) (E_a: 1.97 eV and E_a: 0.41 eV in a sequence). That is, NiFe(111) and PtFe(111) behavior quite differently in promoting demethoxylation of guaiacol to phenol. Moreover, it is noted that H-assisted demethoxylation will lower the activation barrier of CH_β-OCH_3 bond scission with respect to the direct C-OCH_3 bond scission on either NiFe(111) or PtFe(111). In comparison, the promoting effect of H-assisted C-O bond breaking is more pronounced on PtFe(111) than NiFe(111), shown also in previous section. It was reported that on Ru(0001), the dominant guaiacol-HDO to phenol pathway was initiated by the removal of H from hydroxyl OH, followed by methoxyl OCH_3 fully dehydrogenated to form $C_6H_4(O)(OC)$, and then $C_{aryl(\beta)}$-OC breaking occurs to form phenoxy C_6H_4O, and finally H-addition at O to form phenol.[47] Alternative reaction pathway was also reported that started from dehydrogenation of methoxyl OCH_3 to form $C_6H_4(O)(OCH)$, followed by -CH removal to form catecholate $C_6H_4(O)(O)$, and then C_{aryl}–O breaking occurs to form phenoxy C_6H_4O (E_a: 1.10 eV), and finally H-addition at O to form phenol.[49] That is to say, there still exists controversy regarding the favored reaction pathway of guaiacol-HDO to phenol on Ru(0001) regardless of the same DFT approach was employed. We predict that the guaiacol-HDO to phenol on PtFe(111) is more facile than NiFe(111) (E_a: 1.08 eV vs 1.37 eV) and comparable to that on Ru(0001) based on the calculated activation barriers for the RDS.

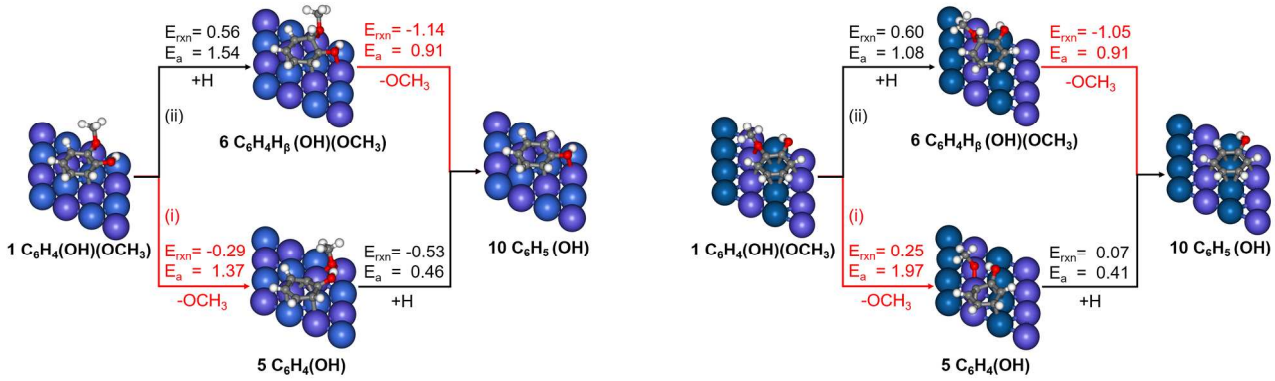

Figure 6. Reaction network for demethoxylation of guaiacol to phenol over (a) NiFe(111) and (b) PtFe(111). Route (i): direct C-OCH_3 bond scission (lower panel); Route (ii): hydrogenation of $C_{aryl(\beta)}$ followed by C-OCH_3 bond scission (upper panel). As in Figure 5.

***3**.2.3 Demethylation of Guaiacol to Catechol.* We lastly examined the two reaction pathways of demethylation of guaiacol to catechol, as shown in Figure 7 and Figure S2. The direct deoxygenation route (i) proceeds via the direct O-CH_3 bond scission to form $C_6H_4(OH)(O)$ (**7**) followed by H-addition at O to yield $C_6H_4(OH)_2$ (**11**), catechol, while the alternative route (ii) contains dehydrogenation of the methoxy OCH_3 to form $C_6H_4(OH)(OCH_2)$ (**8**) followed by O-CH_2 bond scission and hydrogenation to yield catechol. Our results show that Fe-alloying will not compromise the initial dehydrogenation of methoxyl OCH_3 yielding activation barriers of 0.77 eV on NiFe(111) and 0.68 eV on PtFe(111), similar to those on Pt(111) (E_a: 0.75 eV)[45, 46] and Ru(0001) (E_a: 0.64 eV),[47, 49] where $OCH_3 \rightarrow OCH_2$ was also reported as the first step in demethylation of guaiacol to form catechol. Moreover, the subsequent step of O-CH_2 bond scission is more facile on NiFe(111) (E_a: 0.54 eV) and on PtFe(111) (E_a: 0.69 eV) with respect to Pt(111) (E_a: 0.90 eV).[45] This is consistent with the enhanced interactions of O-containing intermediate with oxophilic Fe active surface sites, which serves as a driving force for $C_6H_4(OH)(OCH_2) \rightarrow C_6H_4(OH)(O) + CH_2$ to proceed forward. By contrast, the direct O-CH_3 bond scission to form $C_6H_4(OH)(O)$ (**7**) is less favored as the first step on both alloy surfaces, where it encounters a higher barrier, i.e., E_a: 0.91 eV on NiFe(111) and E_a: 1.51 eV on PtFe(111), followed by the H-addition on the O atom to yield $C_6H_4(OH)_2$ (**11**) (E_a: 1.26 eV and E_a: 0.93 eV, respectively). Hence, the initial dehydrogenation of methoxyl OCH_3 can promote demethylation step of guaiacol on NiFe(111) and PtFe(111). In comparison, route (ii) is favored over route (i) on both alloy surfaces, i.e., E_a: 0.77 eV vs 1.26 eV on NiFe(111) and E_a: 0.68 eV vs 1.51 eV on PtFe(111) for RDS. We predict that the alloying of Fe has little effect on promoting demethylation of guaiacol to catechol, which can be catalyzed on Pt(111), Ru(0001) NiFe(111) and PtFe(111) with similar activity. However, such demethylation steps are not desired in that they do not contribute to promoting any cleavage of C-O bond of guaiacol and the formed catechol can be too stable to proceed for C_{aryl}–OH bond breaking due to its high aromaticity.[45-47, 49] More importantly, carbon content is lost during the process.

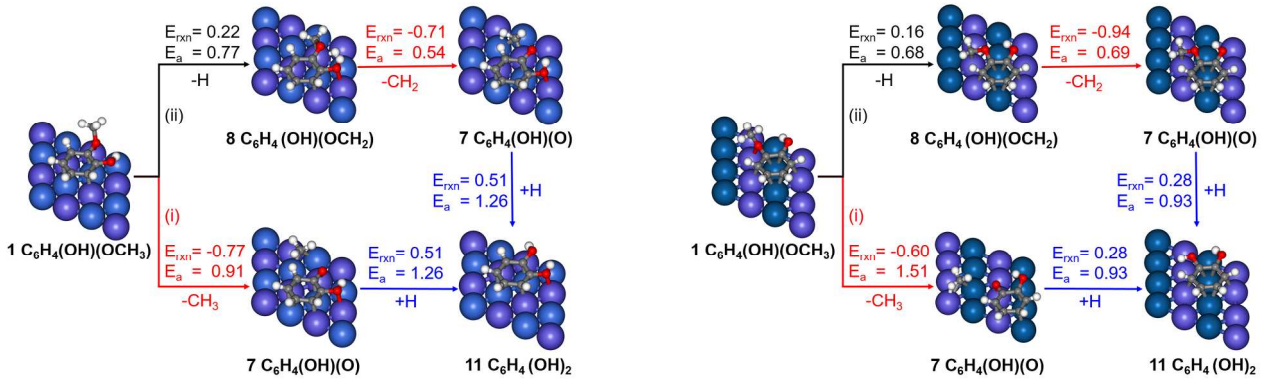

Figure 7. Reaction network for demethylation of guaiacol to catechol over (a) NiFe(111) and (b) PtFe(111). Route (i): direct O-CH_3 bond scission (lower panel); Route (ii): dehydrogenation of the methoxy group followed by O-CH_2 bond scission (upper panel). As in Figure 5.

***3**.2.4 The Most Likely Pathway over NiFe(111) and PtFe(111).* In strict sense, the degree of rate control (DRC) analysis[69, 70] from microkinetic modeling must performed a priori for identifying the rate-determining steps for major product formation from the complex guaiacol-HDO reaction network on bimetallic surface. However, it requires inclusion of full reaction pathway search and parameterization of all reaction constants and thermochemistry, a rather challenging task for large reaction network involving guaiacol-HDO,[31-33, 35-37] which yields numerous intermediate products (e.g., anisole, phenol and catechol) and final products (e.g., benzene, toluene, cyclohexanol, cyclohexanone). This makes the direct comparison of guaiacol-HDO between theoretical modeling and experiments even challenging. Based on the calculated results of a simplified reaction network (Scheme 1), we proposed the most likely pathway for guaiacol-HDO to form anisole, phenol and catechol on NiFe(111) and PtFe(111), as shown in Figure 8. In particular, we focus on the activation mechanism of C_{aryl}–O bond breaking.

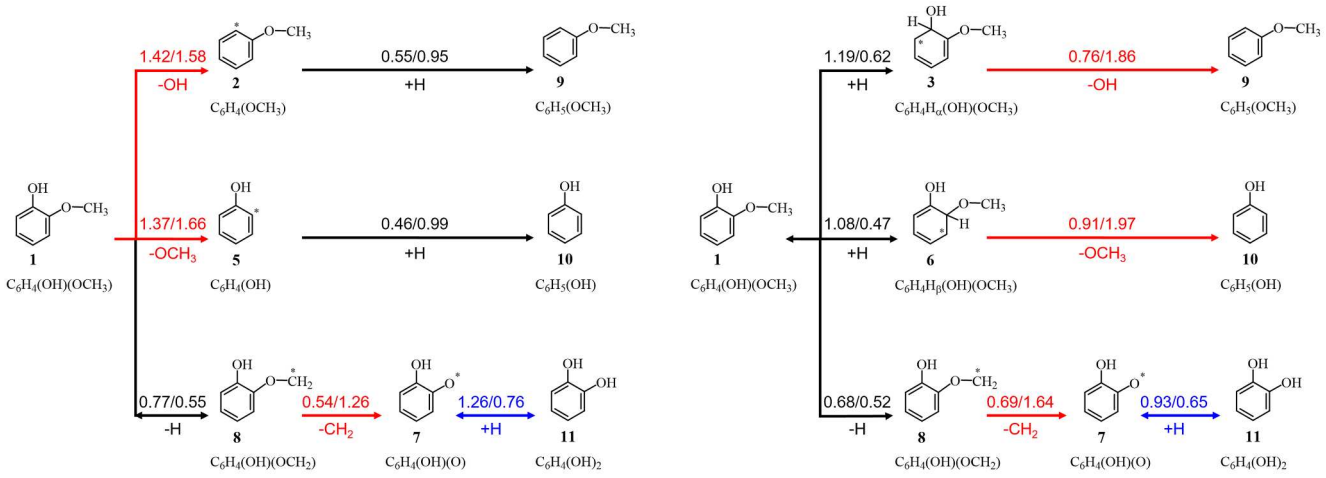

Figure 8. The most likely pathway for hydrodeoxygenation of guaiacol to anisole, phenol and catechol over (a) NiFe(111) and (b) PtFe(111). The values labeled indicate the activation energies (in eV) for forward/reverse reactions estimated using BEP relations. Reversible (irreversible) reactions are indicated by double (single) headed arrows. As in Figure 5.

One can see that the direct C_{aryl}–O bond breaking and dehydrogenation are preferred over hydrogenation on NiFe(111), while hydrogenation/dehydrogenation are preferred over C_{aryl}–O bond breaking on PtFe(111), consistent with the properties of Ni being more oxophilic than Pt regardless of being alloyed with even oxophilic Fe. This is supported by the experimental results that over SiO2-supported Ni catalyst,[36] the deoxygenation products (including benzene) are overwhelmingly dominant over the O-containing aromatics (including phenol, anisole, methoxy-methylphenol), whereas over Pt/TiO2 catalyst,[43] the fully hydrogenated products of cyclohexane and cyclohexanol are dominant over the deoxygenation products regardless of dehydration reactions promoted by acid sites of TiO2. The catalytic consequence can be huge in that guaiacol-HDO is initiated differently by the two alloying surfaces, that is, the direct C_{aryl}–O bond breaking and dehydrogenation on NiFe(111) versus hydrogenation/dehydrogenation on PtFe(111). The most likely deoxygenation pathway is via direct C_{aryl}–O bond scission on NiFe(111) but is via partial H-addition on the aromatic ring followed by $C_{aliphatic}$H-O bond scission on PtFe(111). Based on the calculated activation barriers for the RDS of guaiacol-HDO to anisole, phenol and catechol (i.e., 1.42 eV vs 1.37 eV vs 1.26 eV on NiFe(111) and 1.19 eV vs 1.08 eV vs 0.93 eV on PtFe(111), respectively), the selectivity to catechol is predicted to be higher than phenol and anisole on both Fe-containing alloys. In particular, the removal of oxo-functional group of guaiacol is much easier than monometallic Ni (111) and Pt(111). That is, the direct scissions of $C_{aryl(\alpha)}$-OH, $C_{aryl(\beta)}$-OCH_3 and $C_{aryl(\beta)}$O-CH_3 bonds of guaiacol on PtFe(111) have the activation barriers of 2.05 eV, 1.97 eV and 1.51 eV, respectively, against 2.27 eV (2.40 eV), 2.14 eV (2.44 eV) and 2.00 eV (1.83 eV) on Pt(111),[45, 46] while the direct scission of C-OH bond on NiFe(111) has an activation barrier of 1.23 eV, against 1.89 eV on Ni(111).[26] Among the three model compounds studied, catechol is the major product on either NiFe(111) or PtFe(111), assuming the follow-up reactions do not occur (including those of catechol to phenol, phenol to benzene, anisole to benzene or phenol, full hydrogenation of phenyl ring). Interestingly, catechol has also be identified as the most relevant intermediate in guaiacol-HDO network for phenol and benzene formation on Pt(111)[45, 46] and Ru(0001).[47, 49] This can be explained by the enhanced stability of catechol owing to its high aromaticity, resulting in a higher barrier for C_{aryl}-OH scission as shown in previous studies.[46, 49] In comparison, PtFe(111) is predicted to be better than NiFe(111) in terms of promoting the production of anisole, phenol and catechol with lower activation energies. In other words, superior hydrogenation/dehydrogenation catalyzed by Pt[46] can be critical for providing more feasible pathways for C–O bond breaking besides the direct deoxygenation.

From above, we can see that deoxygenation of guaiacol to form the final aromatic hydrocarbon products must be accompanied with hydrogenation/dehydrogenation *after* or *before* C-O bond breaking as in the case of *NiFe(111)* and *PtFe(111)*, respectively. However, when hydrogenation becomes the dominant elementary step, the efficiency of deoxygenation can be compromised by forming fully hydrogenated alcohols without the removal of O-containing groups. The best scenario is still being the effective direct C-O bond breaking with the minimum hydrogen consumption. Therefore, it is highly desired to identify a good measure for fast screening of highly efficient deoxygenation catalyst for bio-oils upgrading.

3.3 The BEP relations for C-H bond formation and O-H bond scission of phenolic derivatives. The Brønsted–Evans–Polanyi (BEP) relations[71, 72] were initially developed from homogeneous catalysis to describe the linear

relation between the reaction energies (E_{rxn}) and the activation barriers (E_a), but they have been widely applied to analyze surface elementary reaction steps in heterogeneous catalysis.[73] Since then, improved and more advanced BEP relations have been proposed. One of which is the transition state scaling (TSS) relationship that correlates the binding energy (*BE*) of the transition state (TS) with the *BE* of the initial state (IS) or finial state (FS). Several groups, such as Nørskov,[74-76] Vlachos,[17, 45, 77, 78] Hu,[79-81] Sautet,[82] and others[83, 84] have reported the detailed studies of the intrinsic connection between BEP and TSS. The main advantages of applying BEP relations to mechanistic studies are obvious in that the detailed calculations required to locate numerous transition states can be avoided. Hence, if the rate-determining step or the rate-controlling transition state or intermediate is identified according to the DRC analysis on a given reaction network,[85] a fast evaluation of reaction rate and selectivity to a product can be obtained simply from the calculated reaction energy. However, the previous BEP correlations commonly work well for small C1 and C2 open-chain molecules[74-76, 78-81] and are inadequate in estimating the activation barriers of phenolic compounds except for the dehydrogenation of side group (e.g., O-CH_3).

We first present the evidence for the TSS relations for two types of reactions (i) C-H bond formation, (ii) O-H bond scission on monometallic surfaces using methylphenol [$C_6H_4(OH)(CH_3)$], i.e., cresol, as a probe molecule. As shown in Figure 9(a) and (b), a linear correlation can be found in terms of the binding energy of transition state (BE_{TS}) and initial state (BE_{IS}) for C-H bond formation by H-addition to the phenyl ring, regardless of the metal surface, i.e., Ni(111), Pt(111), and Ru(0001) (Table S3). Similar linear correlation can be obtained for O-H bond scission but in terms of the binding energy of transition state (BE_{TS}) and final state (BE_{FS}). Our results of C-H bond formation on Ni(111) agree with previous studies on monometallic surfaces where the linear BE_{TS}-BE_{IS} relations holds for endothermic reactions.[10, 75] In addition, the linear BE_{TS}-BE_{FS} relations for O-H scission on Ni(111) also hold, regardless of whether it is an endothermic process on weaker oxophilic metal surfaces (e.g., Pt) or an exothermic process on moderate to strong oxophilic metal surfaces (e.g., Ni, Ru). While an exothermic process normally follows the linear BE_{TS}-BE_{FS} relations,[10, 76-78, 83] our observed discrepancy may be originated from the strongly polarized nature of the O-H bond and the degree of oxophilicity of the metals. This can be explained by Hammond's postulate[86], which states that the transition state of a reaction resembles either the reactants or the products, to whichever it is closer in energy (i.e., an initial-state-like TS structure in an exothermic step or a final-state-like TS structure in an endothermic step)[10].

We then test the same TSS relations for guaiacol HDO on bimetallic NiFe(111) and PtFe(111) surfaces. As shown in Figure 9(c) and (d), the similar linear correlations can also be identified for (i) C-H bond formation, (ii) O-H bond scission. In the previous study on guaiacol HDO on Pt(111),[45] the linear BEP relations were established using a select group of phenolic compounds including the C-O bond scission in C_{ring}-OA/C_{ring}O-CH_x (A is H or CH_x, x = 1,2) and O-CH_3, as well as O-H bond breaking. Our results suggest that the intrinsic connection between BEP and TSS indeed exist even for elementary steps in complex guaiacol HDO on bimetallic alloy surfaces.

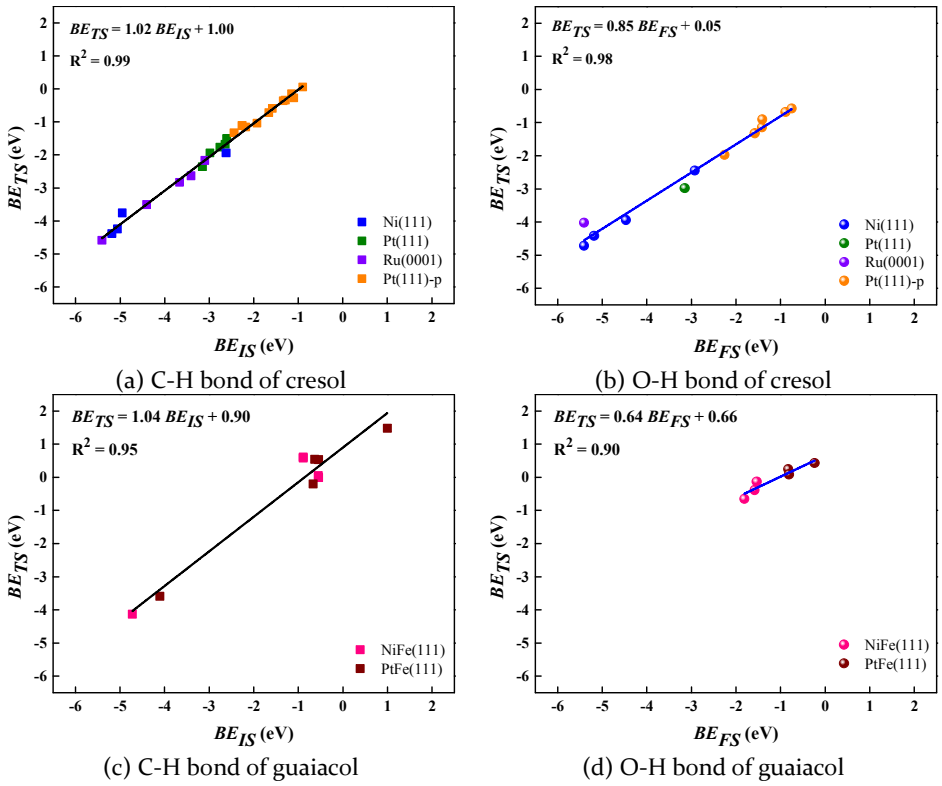

Figure 9. Linear correlation between the binding energy of transition state (BE_{TS}) with initial state (BE_{IS}) or final state (BE_{FS}) for two types of reactions (a) and (c): C-H bond formation (black line); (b) and (d): O-H bond scission (blue line). BE_{IS}, BE_{IS}, and BE_{TS} are calculated using a reference of gas-phase cresol or guaiacol and H_2, which are appropriate for intermediate species. For (a) and (b), some of the data points were retrieved from the literature for m-cresol HDO on Pt(111) and Ru(0001),[20] p-cresol HDO on Pt(111) (denoted as Pt(111)-p),[17] and m-cresol HDO on Ni(111).[26]

3.4. The C-O bond length as a good descriptor for prediction of C-O bond scission reactivity of phenolic compounds. Descriptor-based analysis is a powerful approach for fast catalyst screening and understanding of the trends across the various catalysts for a specific reaction.[87, 88] In essence, a good catalytic descriptor reflects the level of understanding of the atomic-scale details that determines the turn-over-frequency of a given reaction and the selectivity to a target product. Nørskov and co-workers[89, 90] developed a model which uses the linear scaling relationships to estimate all the needed intermediate/transition-state energies from one or two key descriptors, which are typically the adsorption energies of atomic species of C, O and N. They also proposed the electronic descriptor, namely, the d-band center, to describe the structure–activity relationships of transition metals (TMs),[91, 92] which has been recently extended to TM sulfides.[93, 94] Their approach made a significant simplification in the understanding and quantifying of Sabatier volcano, a principle that governors the catalyst activity. More recently, alternative descriptors have been proposed that include the coordination numbers[82] for incorporating structural sensitivity, the elemental bond orders[94] for revealing the origin of the promoting or poisoning effect of nonmetals, and the lattice mismatch[95] for understanding segregation, stability and reactivity of supported thin catalyst films. In most cases, these descriptors work very well in predicting a reaction involved small molecules with simple geometrical structure such as oxygen reduction reaction (ORR)[83] and hydrogen evolution reaction (HER).[82] However, for HDO reaction of lignin-derived phenolic compounds with multifunctional groups bonded to phenyl ring, e.g., guaiacol, the challenges are changed to the selective activation of a specific chemical bond (i.e., C-O

bond) for the removal of O-containing groups accompanied by the minimizing of the activation of other non-oxo functional groups. As such, a high selectivity to desired deoxygenation product can be achieved. Hence, a new descriptor aiming at a fast screening of efficient HDO catalyst is critically needed for relating the activation of C-O bonds to surface active site by using a measurable quantity from the routine DFT calculations.

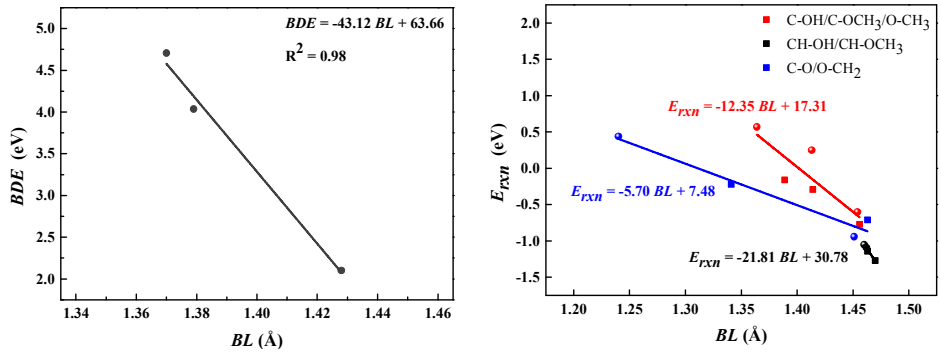

(a) (b)

Figure 10. Energetics for various C-O bond scission reactions as a function of C-O bond length (*BL*). (a) bond dissociation energy (*BDE*)[96] (i.e., C-OH, C-OCH_3, O-CH_3) for gas-phase guaiacol, (b) reaction energy (E_{rxn}).

Table 2. Effects of hydrogenation/dehydrogenation on C-O bond length of adsorbed guaiacol (in Å)[a]

	NiFe(111)		PtFe(111)	
	C1-O1	C2-O2	C1-O1	C2-O2
Adsorption	**1.39**	**1.41**	**1.36**	**1.41**
C-H_α formation	**1.47**	1.45	**1.46**	1.45
C-H_β formation	1.44	**1.46**	1.39	**1.46**
O-H scission	**1.34**	1.41	**1.24**	1.42
H_2C-H scission	1.40	1.37	1.36	1.37

[a]: As in Figure 2(a).

Herein, the C-O bond length (BL) of adsorbed intermediates prior to C-O bond breaking can serve as a good descriptor for predicting C-O bond scission reactivity of the lignin-derived phenolic compounds on similar surfaces. The underlying chemical origin is that the bonding strength of any C-O bonds within a molecule is linearly inversely correlated with C-O bond length, comparable among different molecules with similar bonding situation, as confirmed by the projected crystal orbital overlap population (pCOOP) analysis.[26] Moreover, the C-O bond dissociation energy (*BDE*) of gas-phase guaiacol retrieved from experimental data[96] has a good linear correlation with our calculated C-O bond length as shown in Figure 10(a), consistent with this assessment. For adsorbed guaiacol and its HDO intermediates, the enlargement of C-O bonds can be realized either by means of the electron charge injection into C-O anti-bonding orbitals from the surface activity sites of metal or via hydrogenation/dehydrogenation resulting in transformation of the C(sp^2)-O bond into a C(sp^3)-O aliphatic bond, or vice versa (Table 2). From Figure 10(b), one can see that there exists the linear correlations between reaction energy (E_{rxn}) of C-O bond scission reaction and the C-O bond length (*BL*) for the absorbed guaiacol and its HDO intermediates on NiFe(111) and PtFe(111), forming three distinct groups with varied slope depending on C-O bond scission types in which hydrogenation/dehydrogenation plays a critical role: (i) C-OH, C-OCH_3, and O-CH_3, i.e., $C_{aryl(\alpha,\beta)}$-O or $C_{aryl(\beta)}$O-CH_3 with aromaticity of phenyl ring remained, (ii) CH-OH and CH-OCH_3, i.e., $C_{aliphatic}$H-O with aromaticity of

phenyl ring broken, and (iii) C-O and O-CH_2, i.e., more like C(sp^2)-O due to dangling bond of O and C, respectively. This observation is consistent with our previous study on m-cresol HDO on Ni(111) and NiFe(111),[26] but with a different slope due to the different bonding situation. Our results reveal the trends of C-O bond breakings of guaiacol via either direct or indirect bond scission using C-O bond length as a descriptor. It is suggested that on NiFe(111) and PtFe(111), C-O bond scission reactions become more facile energetically (from endothermic to exothermic) as the activated C-O bond length is enlarged. For example, $C_{aliphatic}$H-O bond breaking [black line in Figure 10 (b)] is much exothermic owing to the prior partial hydrogenation of C_{aryl} of guaiacol, by which C-O bond length is greatly increased.

4. CONCLUSIONS

We have evaluated guaiacol-HDO reaction mechanism on bimetallic NiFe(111) and PtFe(111) using DFT approach. It was found that the direct C_{aryl}–O bond breaking and dehydrogenation are preferred over hydrogenation on NiFe(111), while hydrogenation/dehydrogenation are preferred over C_{aryl}–O bond breaking on PtFe(111). The most likely deoxygenation pathway is via direct C_{aryl}–O bond scission on NiFe(111) but is via partial H-addition on the aromatic ring followed by $C_{aliphatic}$H-O bond scission on PtFe(111). The superior hydrogenation/dehydrogenation catalyzed by Pt is responsible for providing more feasible pathways for C–O bond breaking besides the direct deoxygenation, making PtFe(111) likely to be superior over NiFe(111) in terms of promoting the production of anisole, phenol and catechol with lower activation energies. Deoxygenation of guaiacol to form the final aromatic hydrocarbon products must be accompanied with hydrogenation/dehydrogenation *after* or *before* C-O bond breaking as in the case of *NiFe(111)* and *PtFe(111)*, respectively. Catechol is the major product of guaiacol-HDO on either NiFe(111) or PtFe(111), assuming the follow-up reactions do not occur. In comparison, the removals of oxo-functional group of guaiacol (i.e., $C_{aryl(\alpha)}$-OH, $C_{aryl(\beta)}$-OCH_3 and $C_{aryl(\beta)}$O-CH_3 bond breakings) on both Fe-alloyed surfaces are predicted to be more facile energetically than those on monometallic Ni (111) and Pt(111) owing to oxophilic Fe active surface sites.

Furthermore, two TSS relationships were identified on bimetallic Fe-alloyed surfaces (i) the linear BE_{TS}-BE_{IS} relation for C-H bond formation, (ii) the linear BE_{TS}-BE_{FS} relation for O-H bond scission. Our results suggest that the intrinsic connection between BEP and TSS still holds for elementary steps in complex guaiacol HDO on bimetallic alloy surfaces. Finally, we confirmed that the C-O bond length of adsorbed intermediates can serve as a good descriptor for predicting C-O bond scission reactivity of the lignin-derived phenolic compounds on metal surfaces depending on C-O bond scission types (i) C-OH, C-OCH_3, and O-CH_3, with aromaticity of phenyl ring remained, (ii) CH-OH and CH-OCH_3, with aromaticity of phenyl ring broken, and (iii) C-O and O-CH_2, having C(sp^2)-O bond features. This provides an alternative means for fast screening of highly efficient deoxygenation catalyst for bio-oils upgrading.

Acknowledgements

This work was supported by the National Natural Science Foundation of China (21673137), the "Innovation Action Program" from Natural Science Foundation of Shanghai City (16ZR1413900), the internal fund from Shanghai University of Engineering Science (nhrc-2015-01, 16KY0401). CHT acknowledges partial support from the National Science Foundation (CBET-1510485). The DFT calculations were performed on TianHe-1(A) at the National Supercomputer Center in Tianjin, China, and using computational resources at the Center for Functional Nanomaterials, a user facility at Brookhaven National Laboratory, U.S. DOE facility.

Conflicts of interest

There are no conflicts to declare

Notes and references

1. C. Li, X. Zhao, A. Wang, G. W. Huber and T. Zhang, *Chem. Rev.*, 2015, **115**, 11559-11624.
2. M. Saidi, F. Samimi, D. Karimipourfard, T. Nimmanwudipong, B. C. Gates and M. R. Rahimpour, *Energy Environ. Sci.*, 2013, **7**, 103-129.
3. D. M. Alonso, S. G. Wettstein and J. A. Dumesic, *Chem. Soc. Rev.*, 2012, **41**, 8075-8098.
4. M. Sankar, N. Dimitratos, P. J. Miedziak, P. P. Wells, C. J. Kiely and G. J. Hutchings, *Chem. Soc. Rev.*, 2012, **41**, 8099-8139.
5. C. Liu, H. Wang, A. M. Karim, J. Sun and Y. Wang, *Chem. Soc. Rev.*, 2014, **43**, 7594-7623.
6. C. Zhou, X. Xia, C. Lin, D. Tong and J. Beltramini, *Chem. Soc. Rev.*, 2011, **40**, 5588-5617.
7. A. M. Ruppert, K. Weinberg and R. Palkovits, *Angew. Chem. Int. Ed.*, 2012, **51**, 2564-2601.
8. P. M. de Souza, R. C. Rabelo-Neto, L. E. P. Borges, G. Jacobs, B. H. Davis, D. E. Resasco and F. B. Noronha, *ACS Catal.*, 2017, **7**, 2058-2073.
9. P. M. de Souza, R. C. Rabelo-Neto, L. E. P. Borges, G. Jacobs, B. H. Davis, T. Sooknoi, D. E. Resasco and F. B. Noronha, *ACS Catal.*, 2015, **5**, 1318-1329.
10. A. J. R. Hensley, Y. Wang and J. S. McEwen, *ACS Catal.* , 2015, **5**, 523-526.
11. G. Li, J. Han, H. Wang, X. Zhu and Q. Ge, *ACS Catal.*, 2015, **5**, 2009-2016.
12. R. C. Nelson, B. Baek, P. Ruiz, B. Goundie, A. Brooks, M. C. Wheeler, B. G. Frederick, L. C. Grabow and R. N. Austin, *ACS Catal.*, 2015, **5**, 6509-6523.
13. C. Zhao, W. Song and J. A. Lercher, *ACS Catal.*, 2012, **2**, 2714-2723.
14. Y. Yoon, R. Rousseau, R. S. Weber, D. H. Mei and J. A. Lercher, *J. Am. Chem. Soc.*, 2014, **136**, 10287-10298.
15. C. Zhao, J. He, A. A. Lemonidou, X. Li and J. A. Lercher, *J. Catal.* , 2011, **280**, 8-16.
16. C. Zhao, S. Kasakov, J. He and J. A. Lercher, *J. Catal.*, 2012, **296**, 12-23.
17. G. H. Gu, C. A. Mullen, A. A. Boateng and D. G. Vlachos, *ACS Catal.*, 2016, **6**, 3047-3055.
18. M. B. Griffin, G. A. Ferguson, D. A. Ruddy, M. J. Biddy, G. T. Beckham and J. A. Schaidle, *ACS Catal.*, 2016, **6**, 2715-2727.
19. A. Robinson, G. A. Ferguson, J. R. Gallagher, S. Cheah, G. T. Beckham, J. A. Schaidle, J. E. Hensley and J. W. Medlin, *ACS Catal.*, 2016, **6**, 4356-4368.
20. Q. Tan, G. H. Wang, L. Nie, A. Dinse, C. Buda, J. Shabaker and D. E. Resasco, *ACS Catal.*, 2015, **5**, 6271-6283.
21. C. Chen, G. Y. Chen, F. F. Yang, H. Wang, J. Y. Han, Q. F. Ge and X. L. Zhu, *Chem. Eng. Sci.*, 2015, **135**, 145-154.
22. A. Ausavasukhi, Y. Huang, A. T. To, T. Sooknoi and D. E. Resasco, *J. Catal.*, 2012, **290**, 90-100.
23. L. Nie and D. E. Resasco, *J. Catal.*, 2014, **317**, 22-29.
24. L. Nie, P. M. de Souza, F. B. Noronha, W. An, T. Sooknoi and D. E. Resasco, *J. Mol. Catal. A: Chem.* , 2014, **388-389**, 47-55.
25. A. J. Foster, P. T. M. Do and R. F. Lobo, *Top. Catal.* , 2012, **55**, 118-128.
26. X. Liu, W. An, C. H. Turner and D. E. Resasco, *J. Catal.*, 2018, **359**, 272-286.
27. Q. Tan, G. Wang, A. Long, A. Dinse, C. Buda, J. Shabaker and D. E. Resasco, *J. Catal.* , 2017, **347**, 102-115.
28. X. Zhu, L. L. Lobban, R. G. Mallinson and D. E. Resasco, *J. Catal.*, 2011, **281**, 21-29.
29. Y. Li, J. Fu and B. Chen, *RSC Adv.*, 2017, **7**, 15272-15277.
30. M. A. González-Borja and D. E. Resasco, *Energy Fuels*, 2011, **25**, 4155-4162.
31. R. C. Runnebaum, T. Nimmanwudipong, D. E. Block and B. C. Gates, *Catal. Sci. Technol.*, 2012, **2**, 113-118.

32. T. Nimmanwudipong, R. C. Runnebaum, D. E. Block and B. C. Gates, *Catal. Lett.*, 2011, **141**, 779-783.
33. D. Gao, Y. Xiao and A. Varma, *Ind. Eng. Chem. Res.* , 2015, **54**, 10638-10644.
34. R. N. Olcese, M. M. Bettahar, B. Malaman, J. Ghanbaja, L. Tibavizco, D. Petitjean and A. Dufour, *Appl. Catal., B* 2013, **129**, 528-538.
35. R. N. Olcese, M. Bettahar, D. Petitjean, B. Malaman, F. Giovanella and A. Dufour, *Appl. Catal., B*, 2012, **115**, 63-73.
36. M. V. Bykova, D. Y. Ermakov, V. V. Kaichev, O. A. Bulavchenko, A. A. Saraev, M. Y. Lebedev and V. A. Yakovlev, *Appl. Catal., B*, 2012, **113-114**, 296-307.
37. J. Mao, J. Zhou, Z. Xia, Z. Wang, Z. Xu, W. Xu, P. Yan, K. Liu, X. Guo and Z. C. Zhang, *ACS Catal.* , 2017, **7**, 695-705.
38. N. T. T. Tran, Y. Uemura, S. Chowdhury and A. Ramli, *Appl. Catal., A*, 2016, **512**, 93-100.
39. S. Ansaloni, N. Russo and R. Pirone, *Can. J. Chem. Eng.* , 2017.
40. C. R. Lee, J. S. Yoon, Y. W. Suh, J. W. Choi, J. M. Ha, D. J. Suh and Y. K. Park, *Catal. Commun.*, 2012, **17**, 54-58.
41. X. Zhang, T. Wang, L. Ma, Q. Zhang, Y. Yu and Q. Liu, *Catal. Commun.* , 2013, **33**, 15-19.
42. A. Gutierrez, R. K. Kaila, M. L. Honkela, R. Slioor and A. O. I. Krause, *Catal. Today*, 2009, **147**, 239-246.
43. Z. He, M. Hu and X. Wang, *Catal. Today* 2018, **302**, 136-145.
44. H. Wang, H. Ruan, M. Feng, Y. Qin, H. Job, L. Luo, C. Wang, M. H. Engelhard, E. Kuhn, X. Chen, M. P. Tucker and B. Yang, *ChemSusChem*, 2017, **10**, 1846-1856.
45. K. Lee, G. H. Gu, C. A. Mullen, A. A. Boateng and D. G. Vlachos, *ChemSusChem*, 2015, **8**, 315-322.
46. J. Lu, S. Behtash, O. Mamun and A. Heyden, *ACS Catal.* , 2015, **5**, 2423-2435.
47. J. Lu and A. Heyden, *J. Catal.* , 2015, **321**, 39-50.
48. J. Sun, A. M. Karim, H. Zhang, L. Kovarik, X. Li, A. J. Hensley, J. S. McEwen and Y. Wang, *J. Catal.* , 2013, **306**, 47-57.
49. C. Chiu, A. Genest, A. Borgna and N. Rösch, *ACS Catal.*, 2014, **4**, 4178-4188.
50. V. N. Bui, G. Toussaint, D. Laurenti, C. Mirodatos and C. Geantet, *Catal. Today*, 2009, **143**, 172-178.
51. Y. He and S. Laursen, *ACS Catal.* , 2017, **7**, 3169-3180.
52. G. Kresse and J. Hafner, *Phys. Rev. B*, 1993, **47**, 558-561.
53. G. Kresse and J. Furthmüller, *Phys. Rev. B*, 1996, **54**, 11169-11186.
54. J. P. Perdew, K. Burke and M. Ernzerhof, *Phys. Rev. Lett.*, 1996, **77**, 3865-3868.
55. J. Kibsgaard, C. Tsai, K. Chan, J. D. Benck, J. K. Nørskov, F. Abild-Pedersen and T. F. Jaramillo, *Energy Environ. Sci.*, 2015, **8**, 3022-3029.
56. G. Kresse and D. Joubert, *Phys. Rev. B*, 1999, **59**, 1758-1775.
57. S. Sitthisa, W. An and D. E. Resasco, *J. Catal.*, 2011, **284**, 90-101.
58. B. Fu, W. An, C. H. Turner and G. B. Thompson, *Phys. Rev. Lett.* , 2010, **105**, 096101.
59. Y. K. Takahashi, M. Ohnuma and K. Hono, *Jpn. J. Appl. Phys.*, 2001, **40**, L 1367-L 1369.
60. H. J. Monkhorst and J. D. Pack, *Phys. Rev. B* 1976, **13**, 5188-5192.
61. A. T. Paxton, M. Methfessel and H. M. Polatoglou, *Phys. Rev. B*, 1990, **41**, 8127-8138.
62. G. Henkelman and H. Jónsson, *J. Chem. Phys.* , 1999, **111**, 7010-7022.
63. A. Heyden, A. T. Bell and F. J. Keil, *J. Chem. Phys.* , 2005, **123**, 224101.
64. M. Dion, H. Rydberg, E. Schröder, D. C. Langreth and B. I. Lundqvist, *Phys. Rev. Lett.*, 2004, **92**.
65. J. Klimes, D. R. Bowler and A. Michaelides, *J. Phys.: Condens. Matter*, 2010, **22**, 022201.
66. A. J. R. Hensley, Y. Wang and J. S. McEwen, *Surf. Sci.* , 2016, **648**, 227-235.

67. S. L. Delle, A. Alavi and C. F. Abrams, *Phys. Rev. B*, 2003, **67**, 193406.

68. H. Xin and S. Linic, *J. Chem. Phys.*, 2010, **132**, 221101.

69. S. Maintz, V. L. Deringer, A. L. Tchougreeff and R. Dronskowski, *J. Comput. Chem.*, 2016, **37**, 1030-1035.

70. S. Maintz, V. L. Deringer, A. L. Tchougreeff and R. Dronskowski, *J. Comput. Chem.*, 2013, **34**, 2557-2567.

71. M. G. Evans and M. Polanyi, *Trans. Faraday Soc.*, 1938, **34**, 11-24.

72. J. N. Brønsted, *Chem. Rev.*, 1928, **5**, 231-338.

73. R. A. van Santen, M. Neurock and S. G. Shetty, *Chem. Rev.* , 2010, **110**, 2005-2048.

74. S. Wang, B. Temel, J. Shen, G. Jones, L. C. Grabow, F. Studt, T. Bligaard, F. Abild-Pedersen, C. H. Christensen and J. K. Nørskov, *Catal. Lett.* , 2011, **141**, 370-373.

75. S. Wang, V. Petzold, V. Tripkovic, J. Kleis, J. G. Howalt, E. Skulason, E. M. Fernandez, B. Hvolbaek, G. Jones, A. Toftelund, H. Falsig, M. Bjorketun, F. Studt, F. Abild-Pedersen, J. Rossmeisl, J. K. Nørskov and T. Bligaard, *Phys. Chem. Chem. Phys.*, 2011, **13**, 20760-207605.

76. P. Ferrin, D. Simonetti, S. Kandoi, E. Kunkes, J. A. Dumesic, J. K. Nørskov and M. Mavrikakis, *J. Am. Chem. Soc.* , 2009, **131**, 5809-5815.

77. S. Wang, V. Vorotnikov, J. E. Sutton and D. G. Vlachos, *ACS Catal.* , 2014, **4**, 604-612.

78. J. E. Sutton and D. G. Vlachos, *ACS Catal.* , 2012, **2**, 1624-1634.

79. Z. Liu and P. Hu, *J. Chem. Phys.* , 2001, **115**, 4977-4980.

80. A. Michaelides, Z. Liu, C. Zhang, A. Alavi, D. A. King and P. Hu, *J. Am. Chem. Soc.* , 2003, **125**, 3704-3705.

81. J. Cheng and P. Hu, *J. Phys. Chem. C*, 2008, **112**, 1308-1311.

82. F. Calle-Vallejo, D. Loffreda, M. T. M. Koper and P. Sautet, *Nat. Chem.*, 2015, **7**, 403.

83. H. Wang and W. An, *Catal. Sci. Technol.*, 2017, **7**, 596-606.

84. Y. Xu, A. V. Ruban and M. Mavrikakis, *J. Am. Chem. Soc.*, 2004, **126**, 4717-4725.

85. C. T. Campbell, *ACS Catal.*, 2017, **7**, 2770-2779.

86. G. S. Hammond, *J. Am. Chem. Soc.*, 1955, **77**, 334-338.

87. J. K. Nørskov, F. Abildpedersen, F. Studt and T. Bligaard, *Proc. Natl. Acad. Sci. U.S.A.*, 2011, **108**, 937.

88. M. Salciccioli, M. Stamatakis, S. Caratzoulas and D. G. Vlachos, *Chem. Eng. Sci.* , 2011, **66**, 4319-4355.

89. R. M. Watwe, H. S. Bengaard, J. R. Rostrup-Nielsen, J. A. Dumesic and J. K. Nørskov, *J. Catal.*, 2000, **189**, 16-30.

90. F. Studt, F. Abild-Pedersen, T. Bligaard, R. Z. Sørensen, C. H. Christensen and J. K. Nørskov, *Science*, 2008, **320**, 1320-1322.

91. B. Hammer and J. K. Nørskov, *Surf. Sci.*, 1995, **343**, 211-220.

92. B. Hammer and J. K. Nørskov, *Adv. Catal.*, 2000, **45**, 71-129.

93. C. Tsai, K. Chan, J. K. Nørskov and F. Abild-Pedersen, *J. Phys. Chem. Lett.*, 2014, **5**, 3884.

94. C. Tsai, A. A. Latimer, J. S. Yoo, F. Studt and F. Abildpedersen, *J. Phys. Chem. Lett.*, 2015, **6**, 3670.

95. E. Fako, A. S. Dobrota, I. A. Pašti, N. López, S. V. Mentus and N. V. Skorodumova, *Phys. Chem. Chem. Phys.*, 2018, **20**, 1524-1530

96. A. M. Verma and N. Kishore, *ChemistrySelect*, 2016, **1**, 6196-6205.

TOC

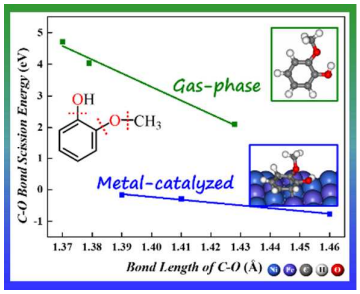

Small means big: DFT-calculated C-O bond length of adsorbed intermediates can serve as a good descriptor for predicting C-O bond scission reactivity of the lignin-derived phenolic compounds over metal catalysts, illustrated by the trends for guaiacol-HDO on bimetallic Fe-alloyed (Ni, Pt) surfaces.